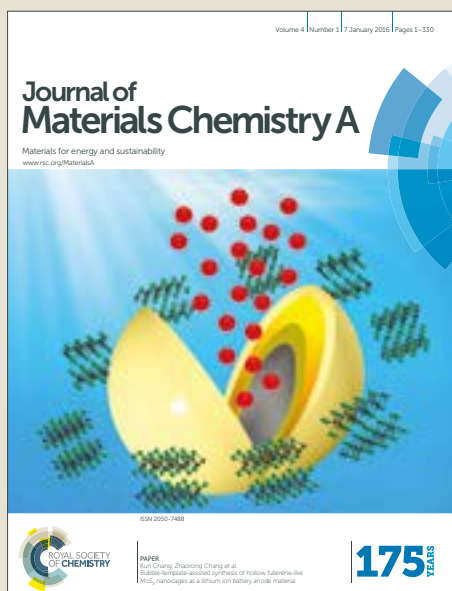


# Journal of Materials Chemistry A

Accepted Manuscript



This article can be cited before page numbers have been issued, to do this please use: Y. Lin, L. He, T. Chen, D. Zhou, L. Wu, X. Hou and C. Zheng, *J. Mater. Chem. A*, 2018, DOI: 10.1039/C7TA09524D.



This is an Accepted Manuscript, which has been through the Royal Society of Chemistry peer review process and has been accepted for publication.

Accepted Manuscripts are published online shortly after acceptance, before technical editing, formatting and proof reading. Using this free service, authors can make their results available to the community, in citable form, before we publish the edited article. We will replace this Accepted Manuscript with the edited and formatted Advance Article as soon as it is available.

You can find more information about Accepted Manuscripts in the [author guidelines](#).

Please note that technical editing may introduce minor changes to the text and/or graphics, which may alter content. The journal's standard [Terms & Conditions](#) and the ethical guidelines, outlined in our [author and reviewer resource centre](#), still apply. In no event shall the Royal Society of Chemistry be held responsible for any errors or omissions in this Accepted Manuscript or any consequences arising from the use of any information it contains.

## ARTICLE

## Cost-effective and environmentally-friendly synthesis of 3D Ni<sub>2</sub>P from scrap nickel for highly efficient hydrogen evolution in both acidic and alkaline media

Received 00th January 20xx,  
Accepted 00th January 20xx

DOI: 10.1039/x0xx00000x

[www.rsc.org/](http://www.rsc.org/)

Yao Lin,<sup>a</sup> Liangbo He,<sup>a</sup> Tao Chen,<sup>a</sup> Dan Zhou,<sup>a</sup> Li Wu,<sup>b</sup> Xiandeng Hou,<sup>b</sup> and Chengbin Zheng<sup>a,\*</sup>

Due to their high abundance and potential to become alternatives to expensive platinum catalysts for large-scale hydrogen production through electrochemical water splitting, transition metal-based catalysts for hydrogen evolution reaction (HER) have attracted intense interest over the past years. Despite tremendous efforts, environmentally-friendly and cost-effective synthesis of transition metal HER catalysts from scrap metal remains a challenge because of their large amounts of impurities. Herein, a simple strategy combining room temperature photochemical vapor generation with low temperature deposition and phosphorization was developed to synthesize 3D Ni<sub>2</sub>P catalyst from either pure nickel salt or bulk scrap nickel. 3D NiO nanoparticles (NPs) were prepared for the first time *via* room temperature photochemical vapor generation and low temperature (160 °C) deposition. Following complete phosphorization at low temperature, the 3D NiO NPs were converted to a highly active 3D Ni<sub>2</sub>P NPs HER catalyst. Owing to its 3D nanostructure, the synthesized Ni<sub>2</sub>P NPs exhibited prominent electrocatalytic performance and excellent stability in both acidic and alkaline media toward the HER with a low overpotential of 69 mV and 73 mV at 10 mA cm<sup>-2</sup>. Moreover, the chemical vapor generation and deposition processes could be precisely controlled and monitored with use of a miniaturized microplasma optical emission spectrometer.

### Introduction

To address the increasing global energy demands and environmental concerns resulting from fossil-fuel combustion, numerous efforts have been devoted to explore efficient catalysts for hydrogen production since hydrogen is regarded as an ideal and renewable energy source with outstanding energy storage density and perfect environmental friendliness. Among the strategies used to produce hydrogen, considerable research efforts have been devoted to electrochemical water splitting because of its unique advantages: unlimited reactant availability, good manufacturing safety, stable output and high product purity.<sup>1–2</sup> Electrochemical water splitting usually requires high-performance electrocatalysts to improve the hydrogen evolution reaction (HER). Although precious metals, particularly Pt catalysts, exhibit high catalytic performance, they are often limited in practical application due to scarcity and high cost. To date, nickel phosphide catalysts with various structures such as hollow Ni<sub>2</sub>P,<sup>3–4</sup> Ni<sub>12</sub>P<sub>5</sub>/Ni<sub>5</sub>P<sub>4</sub> nanoparticles,<sup>5–6</sup> Ni<sub>5</sub>P<sub>4</sub>-Ni<sub>2</sub>P and NiP<sub>2</sub> nanosheets<sup>7–8</sup> and Ni<sub>2</sub>P nanoarrays<sup>9–10</sup>

show excellent catalytic activity toward HER, making them a promising alternative to use of Pt catalysts.

Although hydrothermal, electrodeposition and thermal decomposition methods are currently available for preparation of nanostructured precursors of nickel HER catalysts,<sup>11–14</sup> the need for highly pure nickel salts and organic compounds as the nickel source, as well as the concomitant toxic waste produced, render these methods non-environmentally-friendly and less economical. By contrast, chemical vapor deposition (CVD) can significantly reduce waste production and retains great potential for large-scale production of nickel based catalysts. However, toxic, expensive and unstable nickel carbonyl is required for this process.<sup>14–16</sup> Nickel has been extensively used in the steel and energy industries because of its excellent ductility and corrosion resistance, including production of corrosion-resistant alloys, catalysts and nickel metal hydride batteries.<sup>17–18</sup> During large-scale applications of nickel in industrial engineering, almost half of the extracted nickel is employed only once before being lost either as production waste, directed to landfill, or used as a trace component in recycled iron or copper alloys.<sup>19–21</sup> Thus, it is highly attractive to develop an approach for simple synthesis of nickel HER catalysts from scrap nickel because it not only remarkably alleviates the potential environmental pollution of scrap nickel but also significantly decreases the cost of preparation of nickel HER catalysts. Clearly, the above mentioned methods cannot be used for the preparation of nickel based catalysts from scrap nickel contaminated with

<sup>a</sup> Key Laboratory of Green Chemistry & Technology, Ministry of Education, College of Chemistry, Sichuan University, Chengdu, Sichuan 610064, China \*Email - abin79@163.com

<sup>b</sup> Analytical & Testing Center, Sichuan University, Chengdu, Sichuan 610064, China Electronic Supplementary Information (ESI) available: [details of any supplementary information available should be included here]. See DOI: 10.1039/x0xx00000x

large amounts of impurities. Therefore, it is necessary to efficiently separate nickel from such impurities prior to the preparation of nickel based catalysts. Chemical vapor generation (CVG) is a technique that can convert nonvolatile precursors (usually ionic species) to their volatile species and further transfer them to the gas phase, accomplishing efficient separation of targets from complex matrices.<sup>22</sup> This methodology has been widely adopted as a sample introduction strategy for analytical atomic spectrometry to improve sensitivity and selectivity.<sup>23–24</sup> With such a CVG technique as photochemical vapor generation (PVG), Ni<sup>2+</sup> can be efficiently converted to volatile Ni(CO)<sub>4</sub> and separated from complex impurities in the presence of formic acid and UV irradiation. Such a process has been used for the sensitive detection of nickel in complex samples with advantages of ease of implementation, elimination of chemical reductant and no matrix interference.<sup>25–27</sup> However, to the best of our knowledge, there is no report about the preparation of HER or other catalysts by coupling room temperature PVG to a low temperature CVD and phosphorization process.

Here, for the first time, we introduce a simple conversion strategy with advantages of freedom from multiple synthetic steps and high deposition temperature, which can transform scrap nickel directly to the 3D precursor of Ni<sub>2</sub>P nanoparticles supported on carbon cloth (Ni<sub>2</sub>P NPs/CC).

## Results and discussion

As outlined in Figure 1a, nickel can be efficiently extracted into formic acid solution from scrap nickel through a simple ultrasound-assisted acid extraction. It must be noted that formic acid not only acts a reagent to dissolve nickel, but also serves as a necessary medium for the PVG of Ni. Subsequently, as exhibited in Figure 1b, the solution containing nickel is transported to a PVG reactor for UV irradiation, generating volatile Ni(CO)<sub>4</sub>, which can easily decompose to NiO nanoparticles on carbon cloth (NiO NPs/CC) at low temperature (100–180 °C). According to previous studies,<sup>8</sup> nickel based phosphides can be synthesized via a low temperature phosphorization of NiO based on thermal decomposition of Na<sub>2</sub>HPO<sub>4</sub>.

As can be seen in Figure 1c, the color of the extraction solution gradually turns dark-green with increasing extraction time, consistent with the analytical results obtained by inductively coupled plasma mass spectrometry (ICP-MS) (see Table S1 in Supporting Information (SI)), indicating the mass of nickel in the extraction solution increases with extraction time. The amount of nickel in solution can reach 160 and 210 mg after 4 and 8 h, respectively, demonstrating the feasibility of efficient extraction of nickel from its scrap precursor. Furthermore, it was also found that large amounts of impurities exist in the extraction solution (Table S2) and hinder direct preparation of nickel HER catalyst from scrap nickel by the previously reported methods. An earlier reported miniature microplasma optical emission spectrometer<sup>28</sup>

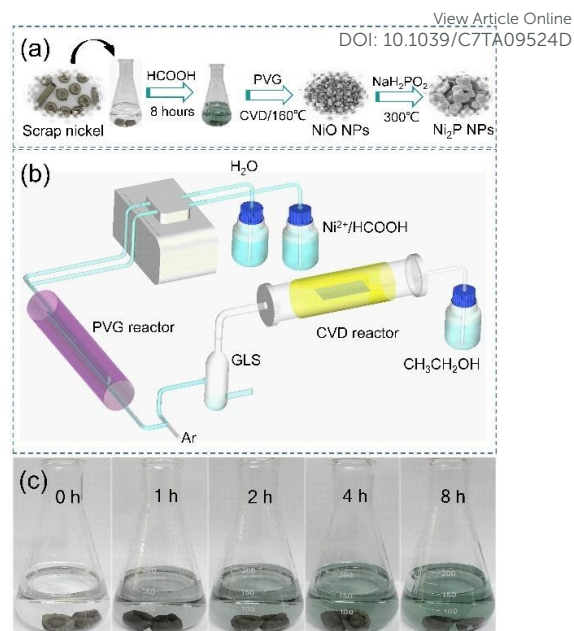


**Figure 1.** (a) Schematic diagram of Ni<sub>2</sub>P NPs/CC preparation via acidic extraction, PVG, low-temperature CVD and phosphorization. (b) A detailed diagram of PVG. (c) Effect of varying extraction time of nickel solution extracted from scrap nickel bulk by ultrasound-assisted dissolution using formic acid.

was utilized to monitor the generation efficiency and CVD efficiency of Ni(CO)<sub>4</sub> via detection of the intensity of the nickel specific atomic emission line before and after the CVD. These processes not only guarantee the efficient generation and deposition of the volatile Ni(CO)<sub>4</sub>, but also warn of any leakage of Ni(CO)<sub>4</sub> to the environment, eliminating this potential threat to the operator. The detailed spectral results are described in Figure S1–S4 of SI.

In order to obtain the optimum temperature for the synthesis of NiO and resultant Ni<sub>2</sub>P NPs/CC, power X-ray diffraction (XRD) was used to investigate the effect of pyrolysis temperature on the phase and structure of the products. As can be seen from Figure 2a, the phase and structure of NiO were remarkably affected by the pyrolysis temperature. There were broad amorphous features and no peaks indicative of crystalline phases at pyrolysis temperatures below 140 °C. The particles began to crystallize and grow in size when the pyrolysis temperature was higher than 140 °C, illustrating that the pyrolysis temperature is critical for the formation of the crystalline precursor. In addition, the diffraction peaks can be mainly attributed to phase-pure NiO (JCPDS card No. 04-0836). Consistently, the NiO NPs obtained at different temperatures also affects the formation of crystalline nickel phosphide. As displayed in Figure 2b, major diffraction peaks at 30.4°, 31.7°, 35.3°, 40.7°, 44.6°, 47.3°, 54.1° and 54.9° index to the (110), (101), (200), (111), (201), (210), (300), and (211) planes of Ni<sub>2</sub>P phase (JCPDS No. 65-1989)<sup>29–30</sup> can evidently be achieved when the temperature is higher than 160 °C. The intensities of

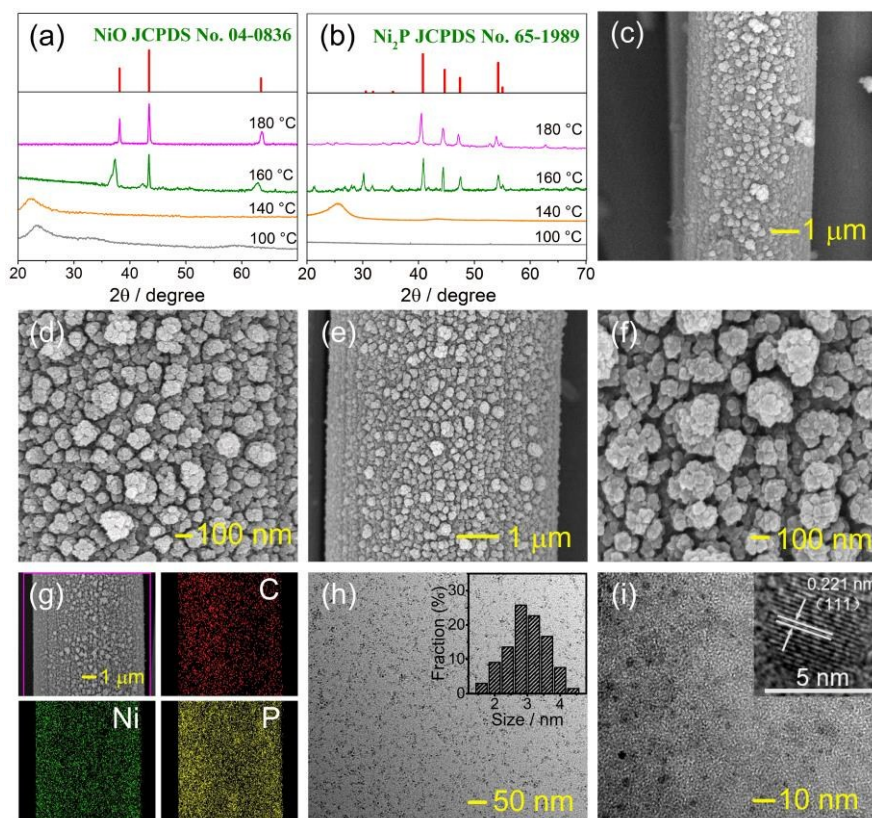


**Figure 2.** XRD patterns of NiO NPs (a) and Ni<sub>2</sub>P NPs/CC (b) prepared at 100, 140, 160 and 180 °C. For comparison, simulated patterns of crystalline NiO and Ni<sub>2</sub>P are also shown at the top. (c) Low- and (d) high-magnification SEM images of NiO NPs/CC prepared at 160 °C. The corresponding (e) low- and (f) high-magnification SEM images of Ni<sub>2</sub>P NPs/CC. (g) SEM and the corresponding element distribution mapping of Ni<sub>2</sub>P NPs/CC. (h) (i) Ni<sub>2</sub>P NPs crystals dispersed on the TEM at different magnifications, (inset: ligament size histogram; the enlarged area of lattice fringes).

the diffraction peaks from NiO NPs become fairly weak after phosphorization, illustrating that complete conversion of nickel oxide to nickel phosphide is achieved at temperatures above 160 °C. To further demonstrate the advantages of PVG, the resultant NiO NPs were dissolved in formic acid and analyzed by ICP-MS. The results (Table S3) reveal that impurities found in the initial extraction solution cannot be detected, indicating that the nickel can be efficiently separated from this complex matrix *via* the PVG process. Thus, the activity of Ni<sub>2</sub>P NPs/CC influenced by impurities was nearly eliminated. The results, summarized in Table S2 and S3, also imply that about 60% of nickel contained in scrap nickel can be utilized to form the NiO.

Scanning electron microscopy (SEM) and transmission electron microscopy (TEM) were employed to study the microstructure of as-prepared catalysts. It is intriguing that the morphology of the NiO NPs consists of relatively regular nanoparticles with 200–300 nm in size (Figure 2c and d). After phosphorization, the surface is composed of relatively loose nanoparticles with a coral-like morphology, as shown in Figure 2e and f. The particle sizes are maintained while a more coral-like structure is obtained. The corresponding elemental mapping images by energy-dispersive X-ray spectroscopy (EDX)

further indicate the well-defined spatial distribution of Ni, P, and C in the basal plane and the incorporation of Ni<sub>2</sub>P coated by carbon cloth (Figure 2g). To further investigate the pyrolysis process, Ni<sub>2</sub>P NPs grown on the CC were exfoliated to solution by sonication and were dispersed on a carbon-coated copper

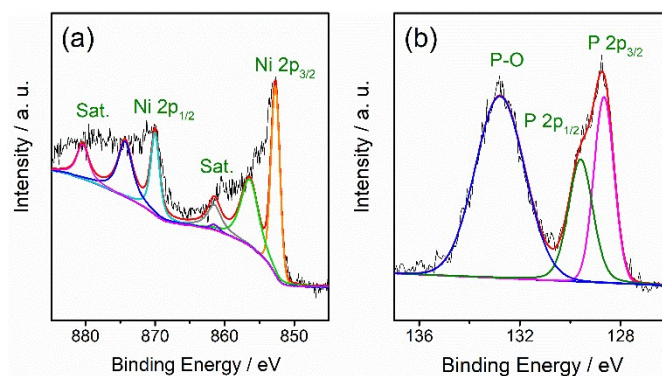


**Figure 3.** (a) XPS spectra of Ni (2p) and (b) P (2p) regions for Ni<sub>2</sub>P NPs/CC. NiO precursors were obtained at 160 °C using an 8 h formic acid extraction solution from scrap nickel, and the Ni<sub>2</sub>P NPs/CC was prepared through a complete phosphorization at 300 °C.

grid for TEM analysis. The TEM image (Figure 2h) shows that large amounts of uniform and well-dispersed crystals with  $3.4 \pm 0.4$  nm in diameter are present. Additionally, the lattice fringe possesses a spacing of 0.221 nm (Figure 2i), corresponding to the XRD peak at  $40.7^\circ$  that belongs to the diffraction of  $\text{Ni}_2\text{P}$ .<sup>3</sup> It is very curious that the  $\text{Ni}_2\text{P}$  NPs can be exfoliated to yield smaller NPs by sonication. We speculate that there are large numbers of pores present in these coral-like  $\text{Ni}_2\text{P}$  NPs. Although the porous structure can be proven with BET characterization, it is not easy to obtain sufficient mass of  $\text{Ni}_2\text{P}$  for the BET characterization because the CVD device was too small to accommodate a larger piece of CC to collect  $\text{Ni}_2\text{P}$  NPs. It is worth noting that as-synthesized  $\text{Ni}_2\text{P}$  NPs/CC are much smaller than previous reports,<sup>3-6</sup> and the interconnected coral-like morphology provides higher contact area, offering more active sites and significantly improving the catalytic activity of the  $\text{Ni}_2\text{P}$  NPs/CC.<sup>31-32</sup>

X-ray photoelectron spectroscopy (XPS) was applied to characterize the state of Ni and P. Figure 3a shows that the high-resolution Ni 2p XPS spectrum can be deconvoluted into two spin-orbit doublets and two shake-up satellites, in which the binding energy for Ni  $2p_{3/2}$  is observed at 852.7 and 856.5 eV, along with one satellite peak at 861.6 eV.<sup>33-34</sup> The Ni  $2p_{1/2}$  spectrum exhibits peaks at 870.2 and 874.3 eV along with a satellite centered at 880.4 eV.<sup>35</sup> The peaks at 852.8 and 870.1 eV are assigned to Ni in the  $\text{Ni}_2\text{P}$  phase, while those at 856.5 and 874.3 eV correspond to  $\text{Ni}^{2+}$  ions possibly interacting with phosphate ions as a consequence of a superficial oxidation.<sup>33,36</sup> The binding energy at 852.7 eV is positively shifted compared to that of Ni metal, indicating the Ni in  $\text{Ni}_2\text{P}$  has a partial positive charge.<sup>33</sup> Figure 3b shows the XPS spectrum in the P 2p region. The peaks located at 128.8 and 129.5 eV are assigned to P  $2p_{3/2}$  and  $2p_{1/2}$  in  $\text{Ni}_2\text{P}$ , respectively,<sup>35</sup> while the peak at 132.7 eV may be attributed to oxidized P species arising from superficial oxidation of  $\text{Ni}_2\text{P}$  due to air contact.<sup>37</sup>

All of the above results confirm that the deposition of  $\text{Ni}(\text{CO})_4$  is an effective means of synthesizing  $\text{Ni}_2\text{P}$ , in which the pyrolysis temperature plays a key role. It is necessary to conduct additional studies to get insight into the relationship between electrochemical HER catalytic activity of  $\text{Ni}_2\text{P}$  NPs/CC and the pyrolysis temperature. Electrochemical HER measurements of the catalysts obtained at various pyrolysis temperatures (100, 140, 160 and 180 °C) were evaluated in acidic (0.5 M  $\text{H}_2\text{SO}_4$ ) and alkaline media (1 M KOH). Impressively, the HER activity of the as-obtained  $\text{Ni}_2\text{P}$  NPs/CC increases successively with the rise of pyrolysis temperature over the range 100–180 °C (Figure 4a and b). Upon increasing the temperature of deposition, the optimal HER activity can be obtained at  $T = 160$  °C, which is consistent with the XRD (Figure 2b) of the synthesized  $\text{Ni}_2\text{P}$ . Moreover, as shown in Figure S5i and l,  $\text{Ni}_2\text{P}$  has a ratio of 2:1 towards Ni and P both at  $T = 160$  °C, which indicated the optimum deposition temperature for the preparation of  $\text{Ni}_2\text{P}$  HER catalyst to be 160 °C. To further evaluate the catalytic activity of these catalysts, a current density of  $10 \text{ mA cm}^{-2}$  was taken into consideration (Figure S6), and the  $\text{Ni}_2\text{P}$  NPs/CC deposited at  $T = 160$  °C was chosen for subsequent investigation.

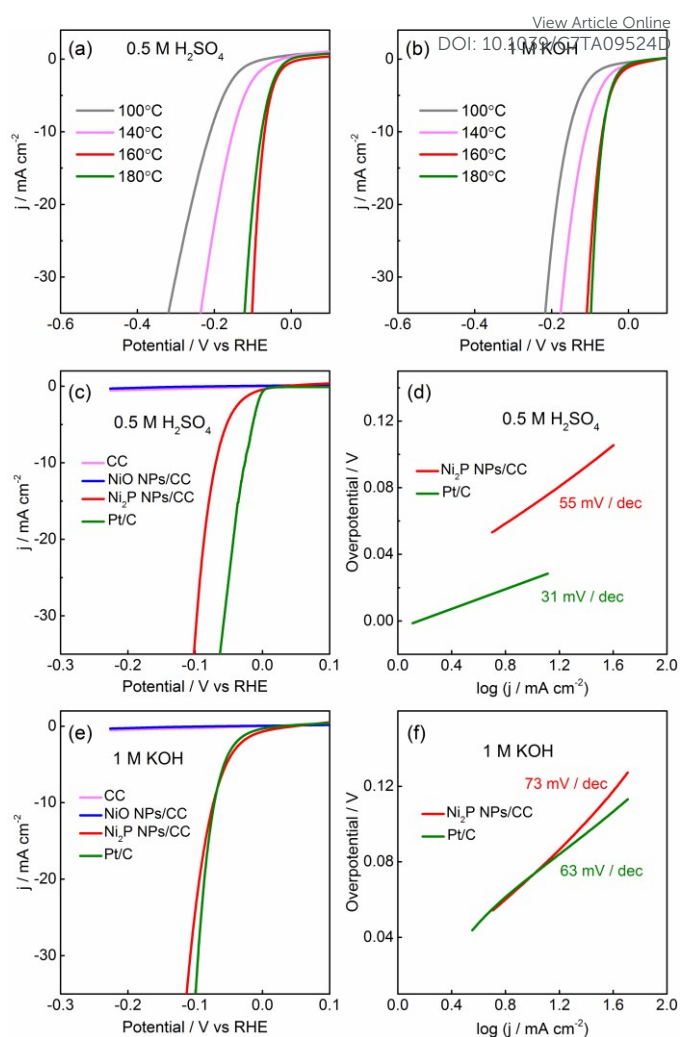


**Figure 4.** Electrochemical HER measurements. Linear sweep polarization curves of obtained  $\text{Ni}_2\text{P}$  NPs in the temperature range 100–180 °C (a) in 0.5 M  $\text{H}_2\text{SO}_4$  and (b) 1 M KOH. Linear sweep polarization curves for CC, NiO and  $\text{Ni}_2\text{P}$  NPs/CC obtained at 160 °C in (c) 0.5 M  $\text{H}_2\text{SO}_4$ , (e) 1 M KOH with a scan rate of  $5 \text{ mV s}^{-1}$ . (d) (f) The corresponding Tafel slopes.

Electrochemical measurements were carefully evaluated in acidic and alkaline media. Commercial Pt/C, NiO NPs/CC and blank CC with the same geometric surface area ( $0.5 \times 0.5 \text{ cm}^2$ ) having a mass loading of  $10.8 \text{ mg cm}^{-2}$  were employed as references (for details see the Experimental Section in SI). In 0.5 M  $\text{H}_2\text{SO}_4$  (Figure 4c), Pt/C catalyst exhibits the expected HER activity with a near zero overpotential. Interestingly, the  $\text{Ni}_2\text{P}$  NPs/CC HER catalyst only required overpotentials of 69 and 134 mV to afford current densities of 10 and  $100 \text{ mA cm}^{-2}$ , respectively, while the CC and NiO NPs/CC present negligible HER activity, indicating the measured activity is attributed to  $\text{Ni}_2\text{P}$  NPs/CC. Although the electrocatalytic current density of  $\eta_{10} = 69 \text{ mV}$  is still higher than that of Pt/C electrode ( $\eta_{10} = 30 \text{ mV}$ ), the catalytic performance of the prepared  $\text{Ni}_2\text{P}$  NPs is comparable to or better than most of the recently reported nickel phosphide electrocatalysts operating in an acidic

medium (See Table S4). The Tafel slope was examined to further estimate the inherent property of this new electrocatalyst. From Figure 4d, Pt yields a Tafel slope of  $31 \text{ mV dec}^{-1}$  as expected.  $\text{Ni}_2\text{P}$  NPs/CC exhibits a small Tafel slope of  $55 \text{ mV dec}^{-1}$  in the overpotential region of 50–100 mV, which is comparable to most of the reported acid-stable nickel phosphide catalysts (Table S4). These data suggest that the HER proceeds through a Volmer-Heyrovsky mechanism and that the electrochemical desorption step is rate-limited.<sup>38-39</sup>

There are, furthermore, few reported nickel phosphides that can be compared to Pt in alkaline media.<sup>40-41</sup> From Figure 4e, we can find that Pt/C represents prominent electrocatalytic activity in 1 M KOH, as expected, with an overpotential as low as 71 mV at a current density of  $10 \text{ mA cm}^{-2}$ . The as-prepared  $\text{Ni}_2\text{P}$  NPs/CC shows an impressively low  $\eta_{10}$  of 73 mV, which compares favorably with Pt/C ( $\eta_{10} = 71 \text{ mV}$ ). Moreover,  $\text{Ni}_2\text{P}$  NPs/CC reveals a small Tafel slope of  $73 \text{ mV dec}^{-1}$  (Figure 4f), which is relatively low compared to reported values for electrocatalysts in alkaline media, and slightly higher than that of Pt/C ( $63 \text{ mV dec}^{-1}$ ). These results also demonstrate  $\text{Ni}_2\text{P}$  retains an efficient Volmer-Tafel mechanism in alkaline media. As shown in Figure S7, the exchange current density ( $j_0$ ) of  $\text{Ni}_2\text{P}$  NPs/CC is calculated to be 0.6158 and  $0.5086 \text{ mA cm}^{-2}$  in  $\text{H}_2\text{SO}_4$  and KOH medium, respectively, as extrapolated from the Tafel plots. Notably, we have proven that the as-fabricated  $\text{Ni}_2\text{P}$  NPs/CC shows slightly lower or similar overpotentials both in basic and acidic media below current densities of  $30 \text{ mA cm}^{-2}$  with excellent HER activity. Further detailed comparisons with other nickel-based phosphide electrocatalysts are presented in Table S4. So far, few electrocatalysts have been reported with good performance in both acid and alkaline conditions owing to their incompatibility.<sup>42-43</sup> In our case, the excellent HER performance of  $\text{Ni}_2\text{P}$  NPs/CC can be potentially due to their smaller size and porous structures.

To further understand the superior HER catalytic activity of  $\text{Ni}_2\text{P}$  NPs/CC, the electrochemically-active surface areas ( $j_{\text{ECSA}}$ ) of the prepared catalysts were investigated. As can be seen from Figure S8,  $\text{Ni}_2\text{P}$  NPs/CC demand overpotentials of 79 and 91 in 0.5 M  $\text{H}_2\text{SO}_4$  and 1 M KOH to deliver a  $\text{HER}_{j_{\text{ECSA}}}$  of  $10 \text{ mA cm}^{-2}$ . Based on the cyclic voltammograms (CVs) (Figure S9), in the region of 0.31 V and 0.41 V (0.5 M  $\text{H}_2\text{SO}_4$ ) and -0.95 and -0.85 V (1 M KOH) vs. RHE, the current response is only due to the charging of the double layer. The capacitances of NiO NPs/CC are calculated to be 4.0 and  $2.62 \text{ mF cm}^{-2}$  in 0.5 M  $\text{H}_2\text{SO}_4$  and 1 M KOH, respectively, with corresponding values of 5.2 and  $7.36 \text{ mF cm}^{-2}$  for  $\text{Ni}_2\text{P}$  NPs/CC, indicating  $\text{Ni}_2\text{P}$  NPs/CC has a higher surface roughness than NiO NPs/CC. Electrochemical impedance spectroscopy (EIS) was also undertaken. The EIS data summarized in Figure S10 suggests that  $\text{Ni}_2\text{P}$  NPs/CC has a smaller semicircle radius than NiO NPs/CC, indicating a much lower  $R_{\text{ct}}$ , and thus a higher charge-transfer rate or more rapid catalytic kinetics.<sup>44</sup> The turnover frequencies (TOFs) of the HER were estimated according to the number of active sites determined from the CV sweep.<sup>45</sup> The surface concentration of redox active sites was extracted from the linear relationship between the reduction peak current and scan rates from CVs (Figure S11). The volume-time curve

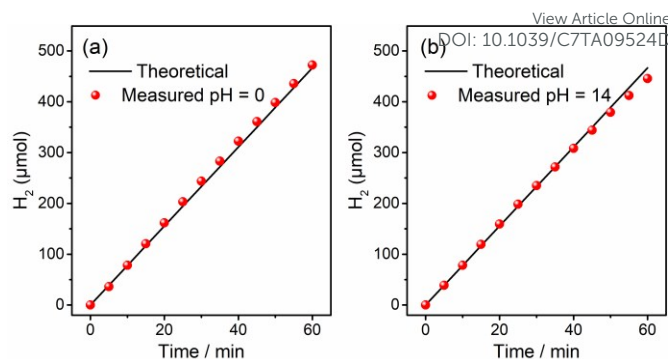


**Figure 5.** The amount of hydrogen gas theoretically calculated and experimentally measured vs. time for  $\text{Ni}_2\text{P}$  NPs/CC in 0.5 M  $\text{H}_2\text{SO}_4$  (a) and 1 M KOH (b).

of the collected  $\text{H}_2$  was nearly the same as the theoretical one calculated according to the cumulative charge (Figure 5), which indicates the Faradic efficiency of the catalyst was nearly 100%. Long-term durability and stability are also critical factors for an HER catalyst. To evaluate these, multiple cycle voltammetric scanning was undertaken between +0.1 and -0.3 V vs. RHE at a scan rate of  $100 \text{ mV s}^{-1}$ . From Figure S12a and b, it is apparent that the polarization curves show negligible degradation after 1000 continuous cycles in acidic and alkaline media, indicating the high stability of  $\text{Ni}_2\text{P}$  NPs/CC under both acidic and alkaline conditions. To further prove the stability, multi-step chronoamperometric curves of  $\text{Ni}_2\text{P}$  NPs/CC were examined with constant current density for 16 h in both cases (Figure S12c and d). The current remains stable in both acidic and alkaline solutions.

## Conclusions

In summary, we have successfully synthesized  $\text{Ni}_2\text{P}$  NPs/CC from bulk scrap nickel through a process of formic acid extraction, photochemical vapor generation, low temperature vapor deposition and phosphorization. The prepared  $\text{Ni}_2\text{P}$  NPs/CC electrocatalyst presents a low overpotential of 69 and 73 at a current density of  $10 \text{ mA cm}^{-2}$  in 0.5 M  $\text{H}_2\text{SO}_4$  and 1 M KOH, respectively, indicating that the catalyst is capable of HER in both acidic and alkaline media. This strategy is simpler, more cost-effective and environmentally-friendlier compared to conventional fabrication methods. Also, it presents a wide range of application for synthesizing multifunctional HER electrocatalysts from readily abundant elements and undoubtedly offers a new avenue for efficient utilization of scrap metal.

## Experimental section

### Synthesis of NiO NPs/CC

As illustrated in Figure 1b, a solution containing nickel chloride and formic acid is transported to a PVG reactor for UV irradiation to generate volatile  $\text{Ni}(\text{CO})_4$ . Nickel solutions obtained by ultrasound-assisted acidic extraction with formic acid were pumped to the PVG reactor. NiO nanoparticle

precursors were obtained by deposition of Ni(CO)<sub>4</sub> at 160 °C, which was generated by subjecting the extracted formic acid solution to UV radiation. The synthesis steps are briefly described as follows: a piece of CC (60 mm × 20 mm) was first washed with concentrated HCl (37%) and then DIW and ethanol to ensure its surface was well cleaned. The extracted Ni<sup>2+</sup> solution, together with formic acid, was pumped into the PVG reactor at a rate of 2 mL min<sup>-1</sup>. Subsequently, volatile Ni(CO)<sub>4</sub> from the gas liquid separator (GLS) was directly transported to the CVD reactor to achieve nickel deposition. The reaction products then flowed into a vessel filled with ethanol to collect any Ni(CO)<sub>4</sub> that escaped. It is noteworthy that the CC was placed in the center of the CVD reactor as a substrate before the deposition. The CVD reactor consisted of a quartz tube tightly wrapped with a polyimide heating film. The size of the quartz tube (80 mm length × 10 mm i.d. × 13 mm o.d.) is much smaller than a traditional CVD tube. The experiments proved that the small tube facilitated deposition of Ni(CO)<sub>4</sub>.

### Synthesis of Ni<sub>2</sub>P NPs/CC

According to a typical methodology, Ni<sub>2</sub>P NPs/CC can be prepared through phosphorization of NiO NPs/CC under an argon atmosphere. The as-obtained NiO and NaH<sub>2</sub>PO<sub>2</sub> powder (0.5 g) were placed at two separate positions in an alumina boat and calcined at 300 °C for 2 h. The mass loading of Ni<sub>2</sub>P NPs was measured to be 10.8 mg cm<sup>-2</sup>.

### Electrochemical measurements

All electrochemical measurements were conducted at room temperature (25 °C) in a typical three-electrode cell. The HER performance was evaluated in 0.5 M H<sub>2</sub>SO<sub>4</sub> (pH = 0.28) and 1 M KOH (pH = 14) solutions using the as-prepared Ni<sub>2</sub>P NPs/CC as the working electrode, a graphite plate as the counter electrode, and a saturated calomel electrode (SCE) as the reference. For comparison, the HER performance of a bare CC and commercially available Pt/C catalyst (1 wt. % Pt) supported on a CC was also measured. Linear sweep voltammetry was applied to obtain polarization curves with a scan rate of 5 mV s<sup>-1</sup>. The stability of as-prepared Ni<sub>2</sub>P NPs/CC was tested at a constant 100 mV.

### Conflicts of interest

There are no conflicts to declare

### Acknowledgements

The authors gratefully acknowledge the National Nature Science Foundation of China (No. 21575092 and 21622508) for financial support.

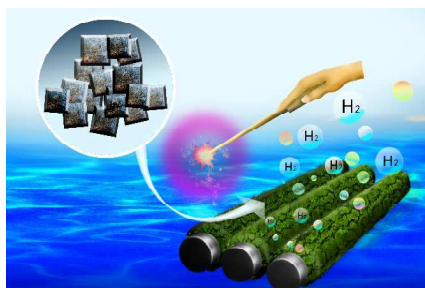
### References

- M. I. Hoffert, K. Caldeira, G. Benford, D. R. Criswell, C. Green, H. Herzog, A. K. Jain, H. S. Kheshgi, K. S. Lackner, J. S. Lewis, H. D. Lightfoot, W. Manheimer, J. C. Mankins, M. E. Mauel, L. J. Perkins, M. E. Schlesinger, T. Volk, T. M. L. Wigley, *Science* 2002, **298**, 981–987. DOI: 10.1039/C7TA09524D
- N. S. Lewis, D. G. Nocera, *Proc. Natl. Acad. Sci.* 2006, **103**, 15729–15735.
- E. J. Popczun, J. R. McKone, C. G. Read, A. J. Biacchi, A. M. Wiltrout, N. S. Lewis, R. E. Schaak, *J. Am. Chem. Soc.* **2013**, **135**, 9267–9270.
- C. Tang, L. Xie, K. Wang, G. Du, A. Asiri, Y. Luo, X. Sun, *J. Mater. Chem. A*, 2016, **4**, 12407–12410.
- A. B. Laursen, K. R. Patraju, M. J. Whitaker, M. Retuerto, T. Sarkar, N. Yao, K. V. Ramanujachary, M. Greenblatt, G. C. Dismukes, *Energy Environ. Sci.* 2015, **8**, 1027–1034.
- Y. Pan, Y. Liu, J. Zhao, K. Yang, J. Liang, D. Liu, W. Hu, D. Liu, Y. Liu, C. Liu, *J. Mater. Chem. A* 2015, **3**, 1656–1665.
- X. Wang, W. Li, D. Xiong, L. Liu, *J. Mater. Chem. A*, 2016, **4**, 5639–5646.
- P. Jiang, Q. Liu, X. Sun, *Nanoscale* 2014, **6**, 13440–13445.
- C. Tang, R. Zhang, W. Lu, Z. Wang, D. Liu, S. Hao, G. Du, A. M. Asiri, X. Sun, *Angew. Chem. Int. Ed.* 2017, **129**, 860–864.
- Y. Bai, H. Zhang, L. Fang, L. Liu, H. Qiu, Y. Wang, *J. Mater. Chem. A*, 2015, **3**, 5434–5441.
- J. F. Callejas, C. G. Read, C. W. Roske, N. S. Lewis, R. E. Schaak, *Chem. Mater.* 2016, **28**, 6017–6044.
- H. Chang, C. Li, M. Yeh, C. Lee, R. Vittal, K. Ho, *J. Mater. Chem. A*, 2014, **2**, 5816–5824.
- E. J. Popczun, C. G. Read, C. W. Roske, N. S. Lewis, R. E. Schaak, *Angew. Chem. Int. Ed.* 2014, **126**, 5531–5534.
- J. F. Callejas, J. M. McEnaney, C. G. Read, J. C. Crompton, A. J. Biacchi, E. J. Popczun, T. R. Gordon, N. S. Lewis, R. E. Schaak, *ACS Nano* 2014, **8**, 11101–1107.
- A. C. Colson, C.-W. Chen, E. Morosan, K. H. Whitmire, *Adv. Funct. Mater.* 2012, **22**, 1850–1855.
- C. Y. Son, I. H. Kwak, Y. R. Lim, J. Park, *Chem. Commun.* 2016, **52**, 2819–2822.
- M. Gong, W. Zhou, M.-C. Tsai, J. Zhou, M. Guan, M.-C. Lin, B. Zhang, Y. Hu, D.-Y. Wang, J. Yang, S. J. Pennycook, B.-J. Hwang, H. Dai, *Nat. Commun.* 2014, **5**, 4695–4701.
- H. Zhang, X. Yu, P. V. Braun, *Nat. Nano* 2011, **6**, 277–281.
- B. K. Reck, T. E. Graedel, *Science* 2012, **337**, 690–695.
- R. B. Gordon, M. Bertram, T. E. Graedel, *Proc. Natl. Acad. Sci.* 2006, **103**, 1209–1214.
- N. Armaroli, V. Balzani, *Angew. Chem. Int. Ed.* 2007, **46**, 52–66.
- R. E. Sturgeon, Z. N. Mester, *Appl. Apectrosc.* 2002, **56**, 202A–213A.
- Z.-a. Li, Q. Tan, X. Hou, K. Xu, C. Zheng, *Anal. Chem.* 2014, **86**, 12093–12099.
- P. Wu, L. He, C. Zheng, X. Hou, R. E. Sturgeon, *J. Anal. At. Spectrom.* 2010, **25**, 1217–1246.
- C. Zheng, L. Yang, R. E. Sturgeon, X. Hou, *Anal. Chem.* 2010, **82**, 3899–3904.
- C. Zheng, R. E. Sturgeon, C. Brophy, X. Hou, *Anal. Chem.* 2010, **82**, 3086–3093.
- Y. Yin, J. Liu, G. Jiang, *Trac Trends Anal. Chem.* 2011, **30**, 1672–1684.
- S. Zhang, H. Luo, M. Peng, Y. Tian, X. Hou, X. Jiang, C. Zheng, *Anal. Chem.* 2015, **87**, 10712–10718.
- L. Guo, Y. Zhao, Z. Yao, *Dalton Trans.*, 2016, **45**, 1225–1232.
- T. Chen, D. Liu, W. Lu, K. Wang, G. Du, A. Asiri, X. Sun *Anal. Chem.* 2016, **88**, 7885–7889.
- B. You, Y. Sun, *Adv. Energy Mater.* 2016, **6**, 1502333.
- H. Wang, S. Min, Q. Wang, D. Li, G. Casillas, C. Ma, Y. Li, Z. Liu, L.-J. Li, J. Yuan, M. Antonietti, T. Wu, *ACS Nano* 2017, **11**, 4358–4364.
- Y. Pan, N. Yang, Y. Chen, Y. Lin, Y. Li, Y. Liu, C. J. Power *Sources* 2015, **297**, 45–52.
- Y. Lu, X. Wang, Y. Mai, J. Xiang, H. Zhang, L. Li, C. Gu, J. Tu, S. C. Mao, *J. Phys. Chem. C* 2012, **116**, 22217–22225.

- 35 Y. Pan, Y. Liu, C. Liu, *J. Power Sources* 2015, **285**, 169–177.
- 36 Z. Pu, Q. Liu, C. Tang, A. M. Asiri, X. Sun, *Nanoscale* 2014, **6**, 11031–11034.
- 37 Y. Pan, Y. Liu, J. Zhao, K. Yang, J. Liang, D. Liu, W. Hu, D. Liu, Y. Liu, C. Liu, *J. Mater. Chem. A* 2015, **3**, 1656–1665.
- 38 Y. Li, H. Wang, L. Xie, Y. Liang, G. Hong, H. Dai, *J. Am. Chem. Soc.* 2011, **133**, 7296–7299.
- 39 X. Wang, W. Li, D. Xiong, D. Y. Petrovykh, L. Liu, *Adv. Funct. Mater.* 2016, **26**, 4067–4077.
- 40 N. Jiang, B. You, M. Sheng, Y. Sun, *Angew. Chem. Int. Ed.* 2015, **127**, 6349–6352.
- 41 Y. Jin, H. Wang, J. Li, X. Yue, Y. Han, P. K. Shen, Y. Cui, *Adv. Mater.* 2016, **28**, 3785–3790.
- 42 J. Yin, Q. Fan, Y. Li, F. Cheng, P. Zhou, P. Xi, S. Sun, *J. Am. Chem. Soc.* 2016, **138**, 14546–14549.
- 43 Y. Zheng, Y. Jiao, Y. Zhu, L. H. Li, Y. Han, Y. Chen, M. Jaroniec, S.-Z. Qiao, *J. Am. Chem. Soc.* 2016, **138**, 16174–16181.
- 44 Z. Peng, D. Jia, A.M. Al-Enizi, A.A. Elzatahry, G. Zheng, *Adv. Energy Mater.* 2015, **5**, 1402031.
- 45 D. Merki, S. Fierro, H. Vrubel and X. Hu, *Chem. Sci.* 2011, **2**, 1262–1267.

View Article Online  
DOI: 10.1039/C7TA09524D

## Table of contents entry



A strategy combining photochemical vapor generation with low temperature deposition and phosphorization was developed to synthesize 3D Ni<sub>2</sub>P HER catalyst